INSTITUT DE FRANCE
Académie des sciences

Comptes Rendus

Géoscience

Sciences de la Planète

Nina J. Jordan, John C. White, Ray Macdonald and Silvio G. Rotolo

Evolution of the magma system of Pantelleria (Italy) from 190 ka to present

Volume 353, Special Issue S2 (2021), p. 133-149

Published online: 31 March 2021
Issue date: 28 January 2022

https://doi.org/10.5802/crgeos.50

Part of Special Issue: Perspectives on alkaline magmas
Guest editor: Bruno Scaillet (Institut des Sciences de la Terre d'Orléans, CNRS, France)

Les Comptes Rendus. Géoscience — Sciences de la Planète *sont membres du Centre Mersenne pour l'édition scientifique ouverte*
www.centre-mersenne.org
e-ISSN : 1778-7025

Comptes Rendus
Géoscience — Sciences de la Planète
2021, 353, nº S2, p. 133-149
https://doi.org/10.5802/crgeos.50

Perspectives on alkaline magmas / *Perspectives sur les magmas alcalins*

Evolution of the magma system of Pantelleria (Italy) from 190 ka to present

Nina J. Jordan [a], **John C. White** [*, b], **Ray Macdonald** [c, d] **and Silvio G. Rotolo** [e, f]

[a] School of Geography, Geology and the Environment, University of Leicester, University Road, Leicester LE1 7RH, UK

[b] Department of Geosciences, Eastern Kentucky University, 521 Lancaster Avenue, Richmond KY 40475, USA

[c] IGMiP, Faculty of Geology, University of Warsaw, al. Zwirki i Wigury 93, 02-089 Warszawa, Poland

[d] Environment Centre, Lancaster University, Lancaster LA1 4YQ, UK

[e] Dipartimento di Scienze della Terra e del Mare, Università di Palermo, Via Archirafi 36, 90123 Palermo, Italy

[f] INGV - Istituto Nazionale di Geofisica e Vulcanologia, Sezione di Palermo, Italy

E-mails: njj5@leicester.ac.uk (N. J. Jordan), john.white@eku.edu (J. C. White), raymacdonald186@gmail.com (R. Macdonald), silvio.rotolo@unipa.it (S. G. Rotolo)

Abstract. The eruptive history of Pantelleria has been marked by the eruption of nine peralkaline ignimbrites, with inter-ignimbrite episodes from small, local volcanic centres. New whole-rock geochemical data are presented for seven ignimbrites and used with published data for younger units to track compositional changes with time. From ~190 ka, silicic magmatism was dominated by comenditic trachyte to comendite compositions, evolving along generally similar liquid lines of descent (LLOD). The final ignimbrite, the Green Tuff (~46 ka), was tapped from a compositionally zoned pantelleritic upper reservoir to a trachytic mush zone. Younger (20–7 ka) silicic magmatism has been relatively small scale, with compositions similar to the earliest pre-Green Tuff pantelleritic ignimbrite (Zinedi). These data suggest that the comenditic reservoirs may have been emplaced at deeper levels than the pantelleritic reservoirs. While both types of series evolved along similar LLOD dominated by fractionation of alkali feldspar, it is the fractionation of iron that determines whether comendite or pantellerite is produced. The deeper reservoirs were more oxidizing and wetter, thus leading to the crystallization of magnetite and therefore the fractionation of iron.

Keywords. Pantelleria, Ignimbrite, Magma reservoirs, Compositional changes with time, Comendite, Pantellerite.

Available online 31st March 2021

* Corresponding author.

1. Introduction

The volcanic island of Pantelleria (adj. Pantescan) has, for the past 40 years or so, been an important focus of petrological and volcanological studies of peralkaline silicic magmatism. It is a small island (83 km^2; Figure 1), for the most part very accessible and with excellent coastal exposures. It consists of a wide range of rock types (basalt, trachyte, comendite, pantellerite), erupted by a variety of mechanisms (lava flows and dome building, pyroclastic falls and flows), and in the pyroclastic units showing very complex lateral and vertical facies changes. Researchers from many institutions internationally have contributed to studies of Pantescan geology. Foremost among the reasons for this interest are the unusual geochemistry (Pantelleria is the type locality for *pantellerite*, a strongly peralkaline, iron-rich rhyolite) and the extremely complex evolutionary history, despite the volcano's youthfulness (~400 ka of subaerial activity). Attempts to evaluate the nature of, and processes within, the plumbing system have been made *via* geophysics [Gianelli and Grassi, 2001, Mattia et al., 2007], geochemical, and thermodynamic modelling [Avanzinelli et al., 2004, Bagiński et al., 2018, Civetta et al., 1984, 1988, 1998, Giuffrida et al., 2020, Liszewska et al., 2018, Neave et al., 2012, Neave, 2020, Romano et al., 2019, White et al., 2005, 2009, 2020], and high P–T experiments [Di Carlo et al., 2010, Romano et al., 2018, 2020]. There is a broad consensus for the presence of an active geothermal system and shallow magma reservoir (at ~4 km depth) which is currently deflating and cooling [Mattia et al., 2007, Civile et al., 2008]. The majority of studies have been made on the Green Tuff ignimbrite (a major marker unit dated at 45.7 ± 1.0 ka; Scaillet et al., 2013), and younger rocks, such that much less is known of earlier units. In this report, we use the Jordan et al. [2018] revision of the pre-Green Tuff stratigraphy and new whole-rock compositional data to examine how the Pantescan magma system may have changed over the period ~190 ka to the present. Detailed petrological studies of the earlier units will be presented elsewhere. A review of the volcanological evolution of Pantelleria is discussed in Rotolo et al. [2021]. We fully appreciate that a critical part of any magmatic system is the input from mafic magmas. Basaltic magmas have always been an important part of Pantescan magmatism and are almost certainly the heat engine that has kept the system active. Here, however, we have concentrated on the silicic magmatism; White et al. [2020] provide an account of the distribution, compositions, and mantle sources of the basalts.

2. Geological setting

The island of Pantelleria lies in the Strait of Sicily, a submerged continental rift between Sicily and Tunisia (Figure 1). Most exposed rocks are felsic, ranging from metaluminous trachyte to peralkaline rhyolite, but mafic magmatism has occurred at several stages in the island's history including the most recent, offshore, eruption in 1891. The oldest documented radiometric date for felsic magmatism is 517 ± 19 ka ($^{40}Ar/^{39}Ar$), from a pantelleritic microgranite inclusion in an ignimbrite [Rotolo and Villa, 2001]. Rotolo et al. [2013] divided the geologic history of the island into three phases. The first phase (~324–190 ka; Mahood and Hildreth, 1986) consists of effusive and explosive activity extensively buried by younger deposits and exposed exclusively along the remote south coast; there are extremely few geochronological or geochemical data available for rocks from this phase. The second phase (~190–46 ka) includes the eruption of eight ignimbrites, ranging in composition from trachyte to comendite/pantellerite, with >20 effusive to strombolian eruptions of pantelleritic magma from small, local centres occurring between the ignimbrite events [Jordan et al., 2018]. The older "La Vecchia" caldera structure on the island formed during this second phase, has been variously dated at 114 ka [Mahood and Hildreth, 1986], between 175 and 133 ka [Speranza et al., 2012], and between 140 and 146 ka [Rotolo et al., 2013]. The third phase began with the 45.7 ± 1.0 ka eruption of the Green Tuff [Scaillet et al., 2013], the caldera-forming ignimbrite of the Cinque Denti caldera, and was followed by a prolonged period of effusive and mildly explosive activity (to ~7 ka; Scaillet et al., 2011).

Jordan et al. [2018] applied formal stratigraphic guidelines, along with detailed field studies, palaeomagnetic data, and $^{40}Ar/^{39}Ar$ ages, to compile a new eruptive history back to the first major ignimbrite eruption, at ~190 ka, the first of eight pre-Green Tuff peralkaline ignimbrites. Ages and descriptions of the eruption units, designated as Formations,

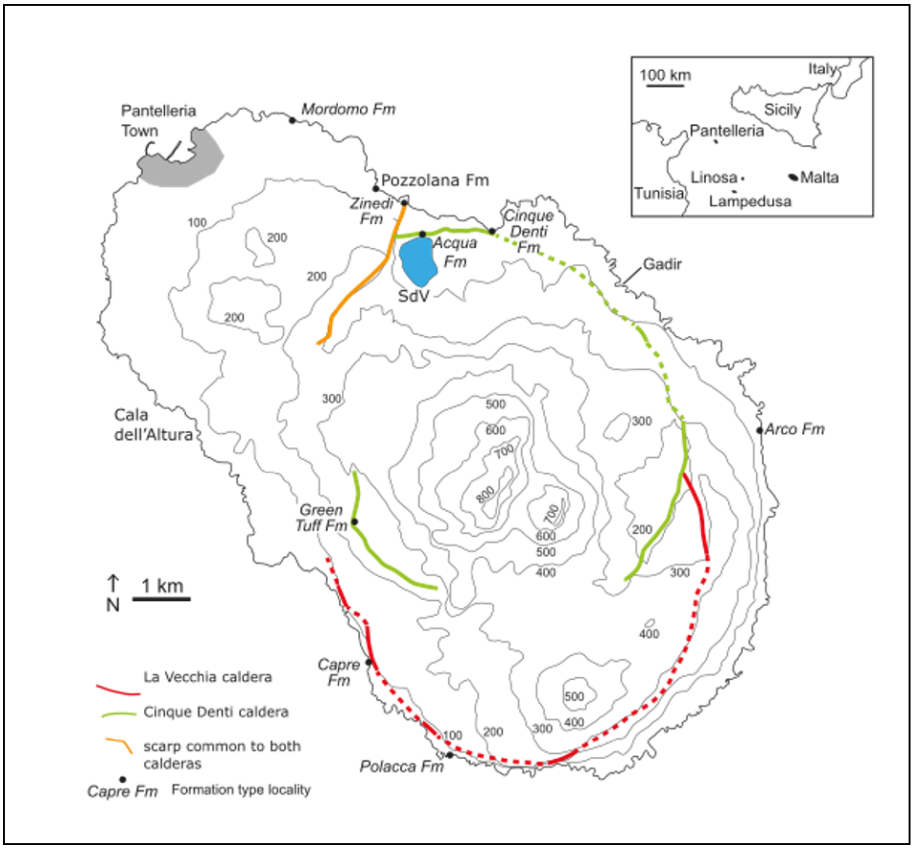

Figure 1. Map of Pantelleria showing topography (CI = 100 m), proposed calderas (after Mahood and Hildreth, 1986), post-caldera faults, type localities of the ignimbrite formations (after Jordan et al., 2018), and selected locations (SdV: Lago Specchio di Venere).

are presented in Table 1 and Figure 2. An important conclusion of their study was that there were at least two and as many as five caldera collapse events associated with the ignimbrite eruptions. The ignimbrites are typically welded and variably rheomorphic and are commonly associated with pumice deposits and lithic breccias, which are interpreted as markers of caldera collapse possibly from reactivated structures [Jordan et al., 2018, Rotolo et al., 2013, 2021]. The onset of eruptions was normally marked by pumiceous air-fall tephra followed by ignimbrite emplacement, which in many cases blanketed the whole island; in one case, the Cinque Denti Formation, pumice fallout followed the ignimbrite emplacement [Jordan et al., 2018]. Jordan et al. [2018] estimated the total onshore volume of all nine ignimbrites, including the Green Tuff, to be 2.32 km^3 DRE, with individual volumes ranging from 0.003 to 0.64 km^3 DRE. They stressed that these are onshore values only because little is known about the amounts deposited at sea. A noteworthy observation is that eruption sizes decreased from 187 to 85 ka, with an increase in the 45.7 ka Green Tuff (Table 1; Figure 3). Inter-ignimbrite periods were characterized by effusive and explosive eruptions from small pumice cones. They are not considered here but it is acknowledged that they could add some complicating details to the evolutionary history of the magma reservoir.

As noted above, Jordan et al. [2018] recognized lithic breccias in several formations as markers of caldera collapse, indicating that they are located close to the inferred source caldera. They also suggested that some collapse events reshaped existing caldera scarps. If calderas can be taken to lie more or less directly above their plumbing systems,

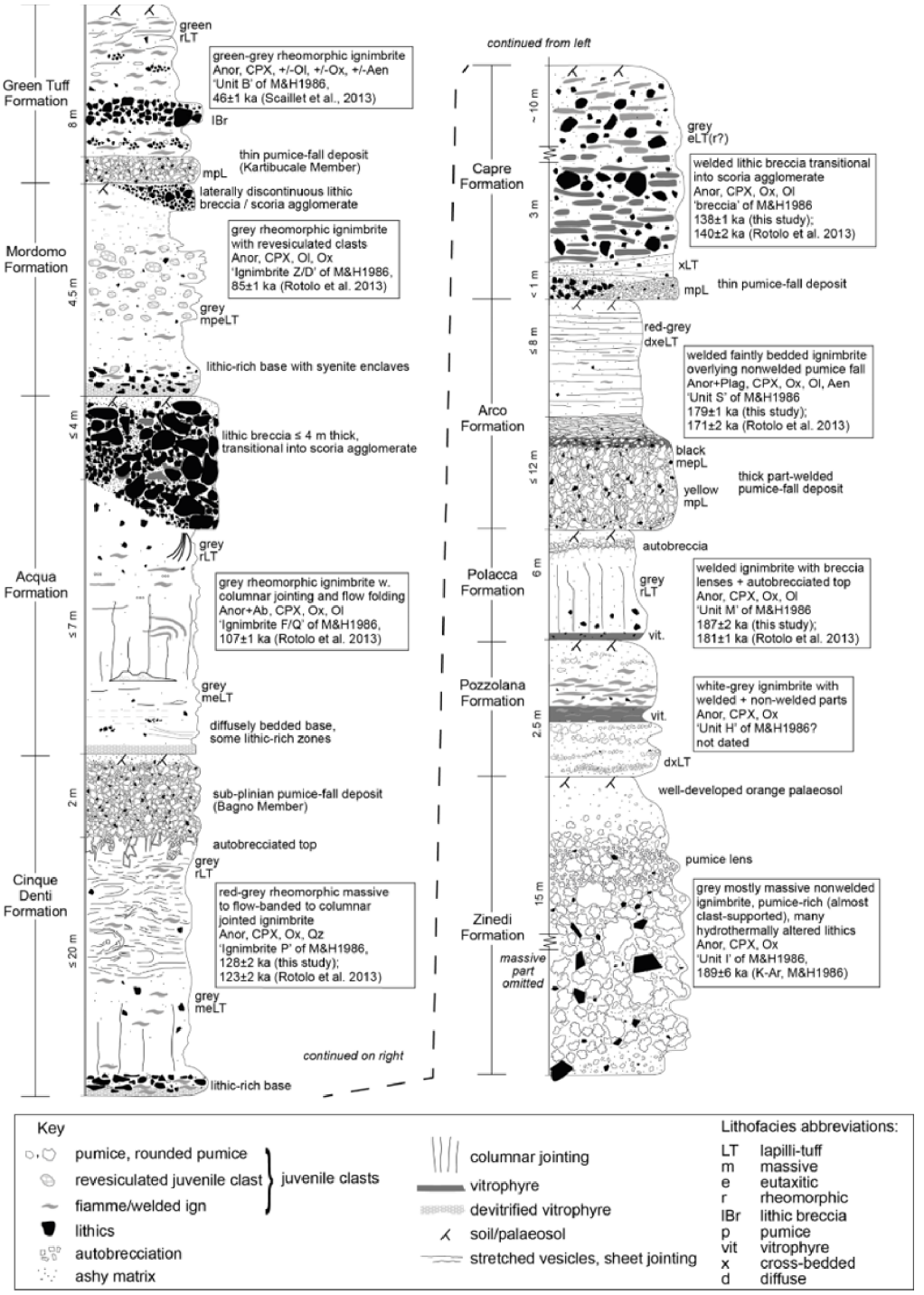

Figure 2. General vertical stratigraphy of ignimbrite-producing eruptions on Pantelleria (not to scale) from Jordan et al. [2018]. Logs are from the type localities of each unit. Abbreviations: M&H86, Mahood and Hildreth [1986]; Anor, anorthoclase; Cpx, clinopyroxene; Ol, olivine; Ox, Fe–Ti oxides; Aen, aenigmatite; Ab, albite; Qz, quartz; Plag, plagioclase.

Table 1. Summary of ignimbrite formations, ages, and geochemistry

Formation	Lat (N)	Long (E)	Age (ka)	Source	*n*	wt% SiO_2	wt% TA	P.I.	wt% FeO^T	wt% Q*	ppm Zr	Zr/Nb	Ce/Y
Green Tuff	36.7750	11.9745	45.7	(1)	36	63.9–71.3	9.8–11.9	1.0–1.8	4.9–8.3	1.3–39.0	291–2061	5.1 ± 0.5	2.6 ± 0.5
Mordomo	36.8375	11.9631	85	(2)	29	65.5–70.3	10.2–11.6	1.0–1.3	4.6–5.8	5.0–22.2	658–1415	5.0 ± 0.5	2.9 ± 0.9
Acqua	36.8191	11.9872	107	(2)	25	64.5–70.8	10.3–12.1	1.1–1.4	4.3–5.7	1.5–24.9	450–1668	5.0 ± 0.3	2.4 ± 0.4
Cinque Denti	36.8200	12.0005	128	(3)	22	65.1–69.4	10.0–13.2	0.9–1.5	3.8–5.7	6.1–19.3	533–1172	5.0 ± 0.1	2.4 ± 0.3
Carpe	36.7533	11.9790	138	(3)	n.d.	n.d.	n.d.	n.d.	n.d.	n.d.	n.d.	n.d.	n.d.
Arco	36.7890	12.0530	179	(3)	8	64.1–72.8	9.8–12.5	1.0–1.4	4.6–6.3	0.4–36.5	481–2173	5.0 ± 0.5	2.6 ± 0.3
Polacca	36.7382	11.9932	187	(3)	8	65.0–66.7	11.5–12.2	1.1–1.2	5.0–5.6	4.1–10.3	397–835	4.9 ± 0.4	2.6 ± 0.2
Pozzolana	36.8265	11.9790	n.a.	n.a.	5	69.7–70.0	10.5–11.8	1.2–1.4	4.8–5.1	22.3–24.9	1616–1783	5.4 ± 0.1	2.5 ± 0.1
Zinedi	36.8242	11.9844	189	(4)	5	66.8–68.0	10.6–11.7	1.1–1.3	6.8–7.9	16.1–21.6	869–1188	4.9 ± 0.1	2.3 ± 0.2

Formation names from Jordan et al. [2018]. Green Tuff data are from Williams et al. [2014] and Liszewska et al. [2018]. Geographic coordinates are for type sections (see Figure 1), datum WGS84. *n* = Number of samples analysed and used in this report. Sources for ages are: (1) Scaillet et al. [2013] $^{40}Ar/^{39}Ar$; (2) Rotolo et al. [2013] $^{40}Ar/^{39}Ar$; (3) Jordan et al. [2018] $^{40}Ar/^{39}Ar$; (4) Mahood and Hildreth [1986] K–Ar. wt% TA = $Na_2O + K_2O$; P.I. = peralkalinity index (mol Na + K/Al); FeO^T, total iron as FeO; wt% Q* = normative Q renormalized to Q + Or + Ab = 100, calculated following Kelsey [1965] with iron oxides calculated following Le Maitre [1976]. n.a., not analysed/not applicable; n.d., no data.

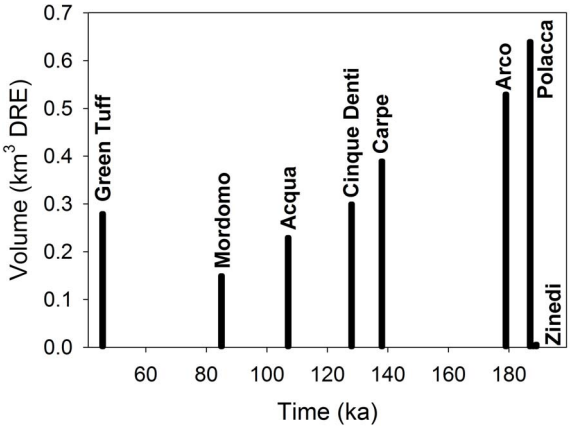

Figure 3. Onshore volumes plotted against eruption ages for the ignimbrite formation (see Table 2; adapted from Jordan et al., 2018).

it seems that the reservoir has been located close to the present reservoir, which geophysical models place at ~4 km below sea level [Mattia et al., 2007]. We assume, therefore, that the magmatic evolution of the island since ~190 ka has been related to one plumbing system, where that system may have varied in its structure and degree of complexity with time.

3. Analytical methods

One hundred and two samples of pre-Green Tuff ignimbrite were collected from Pantelleria during fieldwork from 2009–2012. Representative whole-rock compositional data are presented in Table 2; the full data set is in Supplementary Table 1. Samples were dried at 100 °C overnight, crushed on a flypress to ~2 mm and then milled on an agate planetary mill to a fine powder. For whole-rock samples of ignimbrite, lithic fragments were removed as much as possible during the crushing. Loss on ignition (LOI) was determined in two steps to avoid sample fusion, which renders the powders unusable for bead making. Fusion beads (for major elements) were made from 0.6 g of powder dried following the first step mixed with a flux consisting of 0.6 g lithium tetraborate and 2.4 g lithium metaborate and melted at 1200 °C for 5–10 min. Powder pellets (for trace elements) were made from 6 g of dried powder and 1.5 g of a paraffin wax binding agent at approximately 138 MPa for 30 s. Fused beads and powder pellets were analysed on a Philips PW4400 Axios WD-XRF with a 4 kW rhodium tube at the University of Leicester. The detection limit for major elements is <0.02 wt% and in most cases ~0.003 wt%. For trace elements, detection limits range between 0.1 and 8.2 ppm. Precision, expressed as relative standard deviation across multiple analyses of any given reference material, is typically ~1–3% for major elements (except P_2O_5 and SO_3) and <10% for trace elements (Supplementary Table 2). In terms of accuracy, data obtained at Leicester tend to be slightly higher than the values accepted on the GeoREM database [Jochum et al., 2007].

Table 2. Representative whole-rock analyses

Formation:	Green Tuff	Green Tuff	Mordomo	Mordomo	Acqua	Acqua	Ciqnue Denti	Cinque Denti	Arco	Arco	Polacca	Polacca	Pozzolana	Pozzolana	Zinedi	Zinedi
Sample ID:	150522	160542	300512-4	090612-1	100612-3d	191010-1	BDA1b	250511-2	060612-1	140612-1	310511-1	250912-1a	ukn100d	190610-1	051109-2a	061109-2a
Class:	CT	P	CT	CT	CT	C	MT	CT	CT	P	CT	CT	C	C	PT	PT
SiO_2, wt%	64.68	69.33	65.38	67.74	63.24	69.56	62.62	66.99	61.59	67.66	64.20	66.04	68.52	68.63	63.97	66.03
TiO_2	0.69	0.50	0.66	0.52	0.68	0.44	0.79	0.60	0.74	0.35	0.73	0.63	0.44	0.43	0.64	0.58
Al_2O_3	15.21	9.05	15.30	12.80	15.49	12.33	15.21	13.08	15.47	9.04	15.26	14.40	12.11	11.71	12.33	11.43
$Fe_2O_3^T$	5.88	8.59	5.31	5.71	5.34	5.32	5.60	6.04	4.96	6.55	5.42	5.55	5.27	5.49	7.16	8.50
MnO	0.21	0.29	0.20	0.24	0.22	0.21	0.19	0.24	0.20	0.24	0.21	0.23	0.22	0.24	0.27	0.32
MgO	0.47	0.11	0.43	0.27	0.44	0.31	0.52	0.55	1.01	0.34	0.37	0.38	0.17	0.22	0.53	0.25
CaO	1.23	0.39	0.85	0.52	1.17	0.47	1.77	0.96	1.43	0.29	0.96	0.83	0.41	0.34	0.71	0.67
Na_2O	6.31	6.51	6.92	6.41	6.97	5.43	6.17	5.91	7.05	4.60	6.77	6.87	7.11	5.67	5.47	5.93
K_2O	4.57	4.62	4.58	4.54	4.54	4.72	3.83	4.40	4.00	4.50	4.99	4.55	4.53	5.01	4.57	4.44
P_2O_5	0.15	0.03	0.05	0.05	0.12	0.02	0.08	0.08	0.18	0.02	0.14	0.09	0.04	0.03	0.05	0.04
SO_3	n.a.	n.a.	0.03	0.05	0.31	bdl	0.02	0.01	0.13	0.09	0.03	0.06	0.13	0.04	0.03	0.03
Cl	n.a.	n.a.	0.57	0.59	0.72	0.41	bdl	0.66	1.14	1.23	0.14	bdl	bdl	bdl	0.22	bdl
LOI	0.20	0.10	0.57	1.27	1.73	0.92	1.38	0.82	2.97	5.94	0.33	0.74	1.93	2.90	4.57	1.75
Sum	99.60	99.52	100.86	100.71	100.95	100.14	98.17	100.33	100.88	100.87	99.55	100.37	100.89	100.71	100.53	99.98
O=Cl	n.a.	n.a.	0.13	0.13	0.16	0.09	0.00	0.15	0.26	0.28	0.03	0.00	0.00	0.00	0.05	0.00
Total	99.60	99.52	100.73	100.58	100.79	100.04	98.17	100.18	100.62	100.59	99.51	100.37	100.89	100.71	100.47	99.98
P.I.	1.01	1.74	1.07	1.21	1.06	1.14	0.94	1.11	1.03	1.38	1.08	1.13	1.37	1.26	1.13	1.27
Q*	5.82	34.54	6.25	18.88	2.80	23.40	7.28	16.54	0.40	36.50	5.01	10.25	22.34	24.87	16.09	21.08
Sc, ppm	10.0	3.0	6.5	4.9	9.2	3.4	7.5	4.7	5.5	4.8	7.1	2.6	2.4	4.0	3.7	4.6
V	10.0	13.0	2.3	bdl	bdl	1.6	9.1	7.2	3.4	bdl	2.4	3.0	1.9	1.1	2.0	bdl
Co	1.7	0.2	3.6	3.1	2.4	4.2	5.8	3.0	bdl	2.7	3.2	3.5	2.9	2.9	3.8	3.4
Ni	bdl	bdl	bdl	bdl	bdl	bdl	bdl	4.1	bdl	1.6	bdl	bdl	2.6	2.2	0.7	bdl
Cu	n.a.	n.a.	56.7	58.8	57.7	bdl	0.3	bdl	57.0	61.6	bdl	bdl	3.9	3.6	2.4	bdl
Zn	n.a.	n.a.	146.6	227.4	140.2	222.8	127.9	163.0	131.3	353.7	115.4	171.9	263.7	284.1	208.0	286.1
Ga	31.3	34.7	32.4	34.3	30.8	34.7	28.2	34.2	28.6	33.9	30.9	34.6	35.4	34.9	37.7	40.6
As	n.a.	n.a.	2.5	11.3	1.4	5.4	bdl	2.8	bdl	10.3	bdl	2.4	bdl	bdl	4.8	bdl
Rb	66.0	170.7	77.5	135.4	59.8	144.5	60.8	109.7	57.0	212.3	53.6	83.5	133.5	144.5	96.2	107.6
Sr	65.4	2.8	21.3	13.2	64.3	11.9	240.1	50.0	158.1	11.1	20.1	35.1	12.6	6.8	10.8	19.7
Y	50.5	146.9	44.3	106.6	59.2	95.6	52.5	95.0	51.7	178.7	43.8	77.7	132.8	141.2	92.0	141.3
Zr	552.5	1725.2	658.4	1412.9	449.9	1668.0	533.2	1172.4	523.9	2173.0	396.9	835.1	1616.3	1783.0	868.7	1188.4
Nb	112.1	315.1	146.2	273.0	100.1	325.3	108.6	230.0	110.4	400.1	90.4	172.2	300.8	329.5	180.7	242.1
Mo	n.a.	n.a.	5.6	13.2	6.0	10.7	5.8	5.3	5.6	17.0	5.1	8.9	12.4	19.4	9.4	9.7
Sn	n.a.	n.a.	3.7	9.1	2.5	10.6	bdl	4.3	3.6	16.3	bdl	4.7	bdl	bdl	6.0	bdl
Sb	n.a.	n.a.	bdl	bdl	bdl	bdl	bdl	bdl	bdl	bdl	bdl	1.2	bdl	bdl	bdl	bdl
Cs	0.2	1.8	bdl	7.8	bdl	6.7	bdl	4.3	bdl	16.3	bdl	3.6	10.2	12.5	7.1	8.7
Ba	1893.0	52.0	668.0	142.4	812.8	50.7	1584.2	410.9	1545.6	25.6	903.0	736.6	161.6	119.1	49.0	25.0
La	84.0	212.2	49.8	137.4	68.3	141.8	66.2	134.1	68.0	229.3	53.3	103.3	164.7	181.4	117.9	142.8
Ce	152.4	394.8	96.6	281.4	134.6	301.5	135.7	257.3	135.7	455.8	113.2	210.2	320.3	369.3	223.3	275.5
Nd	67.3	153.7	44.6	108.3	62.4	107.6	53.8	115.4	58.1	175.6	48.8	86.3	125.4	138.1	99.8	119.2
W	n.a.	n.a.	2.4	3.5	1.5	bdl	bdl	2.3	bdl	9.4	1.4	1.6	bdl	bdl	bdl	bdl
Pb	n.a.	n.a.	6.6	10.3	4.9	10.0	6.2	5.7	5.6	15.0	4.1	7.6	10.6	12.9	7.4	8.5
Th	10.8	32.3	9.6	24.1	6.5	28.6	8.1	19.8	9.0	37.5	6.3	13.7	28.2	31.6	14.7	19.7
U	1.3	10.2	2.4	6.2	2.2	6.2	2.8	2.5	2.6	10.8	2.6	3.8	8.4	8.6	4.5	5.1

Full results for pre-Green Tuff Formations are in Supplementary Table 1. Representative Green Tuff samples are from Liszewska et al. [2018]. Class (following Le Maitre 2002; Macdonald 1974): MT, Metaluminous Trachyte; CT, Comenditic Trachyte; C, Comendite; PT, Pantelleritic Trachyte; P, Pantellerite. $Fe_2O_3^T$, total iron as Fe_2O_3. LOI, Loss on Ignition. P.I., peralkalinity index (= mol [Na + K]/Al). Q* = normative quartz renormalized to Q + Or + Ab = 100, calculated following Kelsey [1965] with iron oxides adjusted following Le Maitre [1976]. n.a., not analysed; bdl, below detection limit. Sample BDA1b collected by Rebecca Williams.

4. Significance of the Green Tuff

The Green Tuff is a very remarkable deposit; along with the post-caldera trachytes, it has provided our most complete insight into processes in the Pantescan plumbing system. The eruption had the largest drawdown, penetrating a feldspar-rich crystal mush, subsequently erupted as the post-caldera trachytes

[White et al., 2009]. It contains a complete spectrum of compositions from metaluminous trachytes to the most-evolved (pantellerite) melts yet recorded on the island (~10 wt% FeO^T, 5–3 wt% Al_2O_3, P.I. [peralkalinity index; mol (Na + K)/Al] = 2.61; Liszewska et al., 2018). The trachytes show strong textural disequilibrium, perhaps related to thermal and compositional inputs from more mafic magmas [Ferla and Meli, 2006, Liszewska et al., 2018]. Direct evidence of magma mixing processes occurs in a small lava flow of benmoreite capping the post-caldera trachytes on Montagna Grande [Romengo et al., 2012]. Using olivine compositions, Romengo et al. [2012] raised the possibility that the trachytes may have evolved along with more than one liquid line of descent (LLOD). A suite of syenodioritic xenoliths in the trachytes also point to the presence in the system of melts of intermediate composition [Ferla and Meli, 2006]. In an innovative approach to eruptive dynamics, Williams et al. [2014] used Zr contents as stratigraphic markers to show that the pyroclastic flow member was deposited from a complex diachronic distribution of density currents. High-resolution analysis of the architecture of the deposit provided new insights into how the flow dynamics evolved. During eruption, mingling between layers, especially in the pantellerites, was ubiquitous, at scales down to the micrometer level, a process revealed only by detailed analysis of within-sample glasses, the first record of such intimate mixing in a peralkaline system [Liszewska et al., 2018].

Thermodynamic modelling and experimental studies have provided precise estimates of conditions within the reservoir. From the bottom to the top of the magma reservoir, temperatures decreased from 900 to 700 °C, oxygen fugacity (fO_2) increased from ΔFMQ-1.5 to ΔFMQ-0.5, and silica activity relative to quartz saturation ($a SiO_2$[Qtz]) increased from 0.74 to 1.00 [Di Carlo et al., 2010, Liszewska et al., 2018, Romano et al., 2018, 2020, White et al., 2005, 2009]. The change in oxygen fugacity has been interpreted by these authors as reflecting a roofward increase in water content in the magma. However, evidence from melt inclusions revealed nearly identical concentrations of ~4 wt% H_2O from the middle and base of the Green Tuff section, but with much lower concentrations (~1.2 wt% H_2O) in the comenditic trachyte top of the section [Lanzo et al., 2013, Romano et al., 2019] and may also reflect an increase of $Fe^{3+}/\Sigma Fe$ due to increasing peralkalinity [Stabile et al., 2017]. Finally, using data from olivine zoning in basalts, Giuffrida et al. [2020] suggested that eruption of the Green Tuff and collapse of the Cinque Denti caldera had a profound influence on the internal structure of Pantelleria. For example, the supply of magma from deep crustal storage zones decreased after the eruption, while the dynamics of magma transfer in the upper parts of the plumbing system were enhanced.

5. Geochemistry of the pre-Green Tuff Formations

The rocks of the pre-Green Tuff Formations range from metaluminous (P.I. = 0.94–0.99) to peralkaline (P.I. > 1.0). All units plot together on the total-alkalis silica (TAS) diagram (Figure 4a; Le Maitre, 2002), with trachyte being the dominant rock type. In contrast with the Green Tuff, most of the pre-Green Tuff peralkaline types lie in a cluster straddling the comenditic trachyte–comendite boundary on the FeO^T–Al_2O_3 classification diagram (Figure 4b; Macdonald, 1974). Some analyses from the Zinedi and Arco Formations plot just within the pantellerite field. Harker diagrams (Figure 5) show that comenditic trachytes (~64 wt% SiO_2) from each suite are broadly similar with respect to major element compositions (~0.7 wt% TiO_2, ~15.3 wt% Al_2O_3, ~5.4 wt% FeO^T, ~6.7 Na_2O). With increasing SiO_2 contents, there are decreases in TiO_2, Al_2O_3, CaO, and Na_2O for all suites, with Al_2O_3 decreasing more rapidly in the Green Tuff and Zinedi formations. K_2O shows approximately unchanging behaviour in all formations. For nearly all of the pre-Green Tuff Formations, FeO^T also demonstrates little variability, decreasing slightly at higher SiO_2 in contrast to the Green Tuff and Zinedi Formations, which show iron-enrichment trends.

SiO_2 is plotted against three other compositional parameters in Figure 6. In all formations, peralkalinity increases with increasing SiO_2, with the more rapid decrease of Al_2O_3 in the Green Tuff resulting in overall higher peralkalinity. Figure 6b plots SiO_2 versus $1.33 \cdot FeO^T/(Al_2O_3–4.4)$ [hereafter labelled Fe^T/Al], which has a value of 1.0 along the pantelleritic–comenditic boundary seen in Figure 4b; the trachyte–rhyolite boundary occurs at 69 wt% SiO_2 (Figure 4a). This figure more clearly shows the variation in FeO^T relative to Al_2O_3 with increasing SiO_2

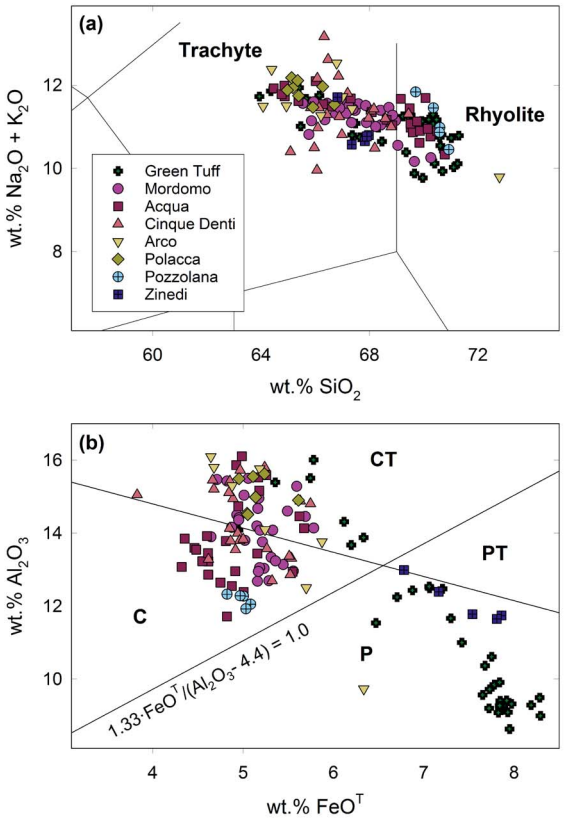

Figure 4. Geochemical classification of the ignimbrites on the (a) total-alkali silica (TAS; Le Maitre, 2002) diagram and on the (b) Macdonald [1974] classification scheme for peralkaline silicic rocks. Green Tuff whole-rock data are from Liszewska et al. [2018] and Williams et al. [2014]. Pre-Green Tuff data are presented in Supplementary Table 1.

and provides a comprehensive classification scheme consistent with Le Maitre [2002] which we adopt for use in Table 2 and Supplementary Table 1. This plot also shows that, unlike the Green Tuff and Zinedi Formations that have relatively rare comenditic trachyte compositions, comenditic trachyte is the dominant rock type in the pre-Green Tuff Formations, and it evolves towards comendite with only a slight increase in Fe^T/Al. In all formations, there is a generally strong positive correlation and range of values between SiO_2 and Zr (Figure 6c). Normative quartz (Q*) renormalized to quartz (Q) + orthoclase (Or) + albite (Ab) = 100 is presented in Figure 6d. This parameter is used to quantify silica-oversaturation as the LLOD moves from the feldspar join (Q* = 0) in the system Q–Or–Ab to a minimum composition on the feldspar–quartz cotectic. To determine these values, iron oxides were adjusted following Le Maitre [1976] and CIPW norms for whole-rock analyses were calculated using the method of Kelsey [1965]. This plot clearly shows that although least-evolved (~64 wt% SiO_2) comenditic trachyte in all formations is close to quartz saturation, Q* in the pre-Green Tuff formations (except Zinedi and Arco) is significantly lower with increasing SiO_2. Because there is an inverse relationship between silica activity and pressure [Nicholls et al., 1971], this may reflect deeper-seated magma chambers for the comenditic trachyte–comendite formations and shallower magma chambers for the comenditic trachyte–pantellerite formations. This is supported by the experimental work of Tuttle and Bowen [1958], Johannes and Holtz [1996], Wilke et al. [2017], and others who document a strong negative correlation between the maximum value of Q* on the feldspar–quartz cotectic and pressure.

Incompatible trace element ratios are remarkably similar for all units (Figure 7 and Table 1), which suggests that throughout the 190 ka history discussed here the felsic magmas evolved from a similar type of basalt. A common basaltic origin for these rocks is also supported by similar patterns observed in multi-element variation diagrams (Figure 8, normalized to depleted MORB mantle [DMM]; Salters and Stracke, 2004), which are nearly identical in shape to each other and to a representative sample of the low Ti–P, pre-Green Tuff basalt shown in Figure 8a (sample 130911; White et al., 2020) with the exception of the compatible trace elements Ba, Sr, P, and Ti, which may reflect fractionation of feldspar, apatite, and Fe–Ti oxides [cf. Civetta et al., 1998, Neave et al., 2012, White et al., 2009]. For a given concentration of Zr, Sr and Ba are higher in the Mordomo, Cinque Denti, and Arco Formations than the others although they all converge to similar levels at >1500 ppm Zr. The elevated Sr and Ba concentrations in these rocks may suggest a significant role for accumulation of alkali feldspar in these rocks. From basalt to comenditic trachyte, all trace elements in Figure 8 show a similar magnitude of increase, with the exception of P, Sr, and Ti, suggesting these trachytes were derived from basalt via fractionation of plagioclase, Fe–Ti oxides, and apatite. From comenditic trachyte to pantellerite, most elements continue to increase

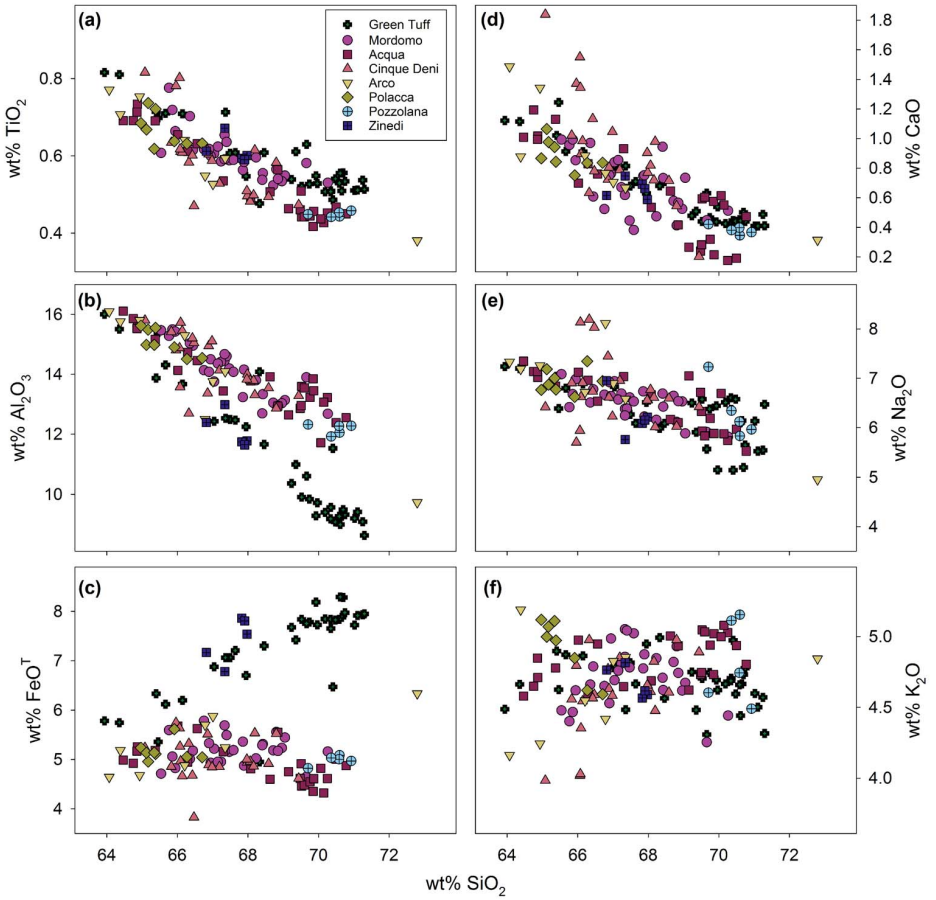

Figure 5. Major element variation diagrams for whole-rock data from the ignimbrites (see Supplementary Table 1). Green Tuff whole-rock data are from Liszewska et al. [2018] and Williams et al. [2014].

with the exception of K, which shows nearly constant behaviour (cf. Figure 5f), Ti (which decreases slightly), P (apatite fractionation) and Sr and Ba, reflecting a dominant role of alkali feldspar fractionation in the formation of both comendite and pantellerite from comenditic trachyte. The trends are similar to those reported in previous studies of Pantescan suites [Civetta et al., 1998, Liszewska et al., 2018, Neave et al., 2012, White et al., 2009]. The petrology of individual ignimbrite formations is the subject of ongoing investigations.

Coexisting basalt–comendite and basalt–pantellerite series have been documented in other intraplate settings, such as the Boseti volcanic complex, Ethiopia [Ronga et al., 2009], Changbaishan, China–North Korean [Andreeva et al., 2019], and Terceira, Azores [Mungall and Martin, 1995]. At Terceira, Mungall and Martin [1995] observed that magnetite is the dominant Fe–Ti oxide (>2.5 vol%) in the basalt–comendite series, whereas ilmenite (s.s. with low haematite component) is the dominant oxide (0.4 to 0.6 vol%) in the basalt–pantellerite series. The same seems to be true at Pantelleria: although ilmenite is the dominant or sole oxide phase in the pantellerites [White et al., 2005, 2009], magnetite (s.s. with high ulvöspinel component) is the dominant or sole oxide phase in the comendites [Jordan, 2014]. Experimental studies have shown that fO_2 exerts a strong control on oxide crystallization, with more reducing conditions favouring ilmenite and more oxidizing conditions favouring magnetite [Ishihara, 1977, Toplis and Carroll, 1995], and also favouring fayalitic olivine over clinopyroxene [Romano et al., 2018]. At Terceira, Mungall and Mar-

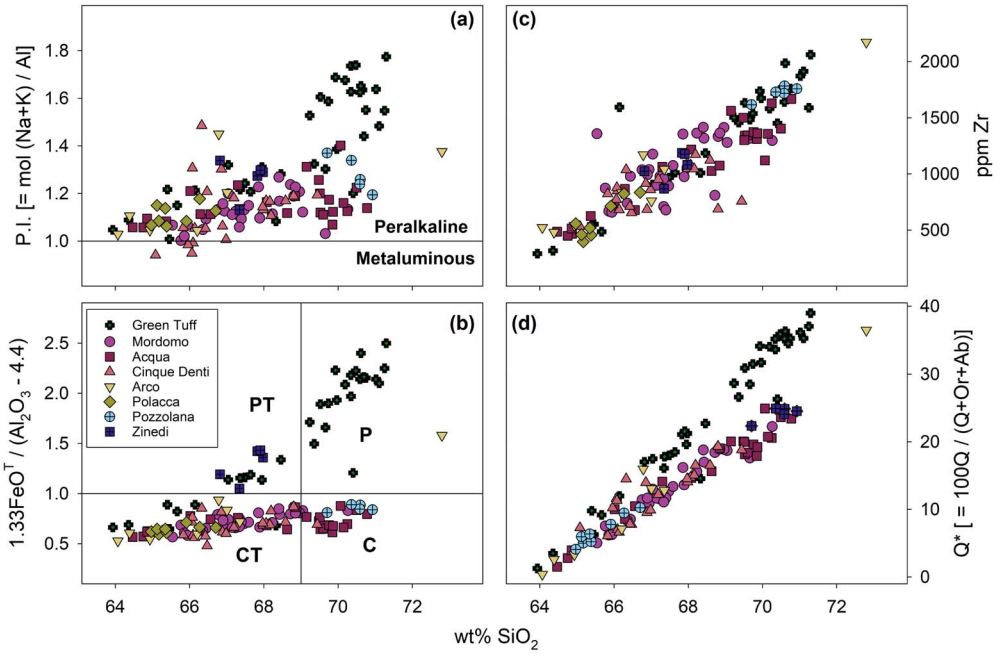

Figure 6. Variation of SiO_2 with (a) the peralkalinity index [P.I.]; (b) relative variability of FeO^T and Al_2O_3 (adapted from Macdonald, 1974); (c) concentration of Zr; and (d) silica-oversaturation, as Q* = $100 \cdot Q/(Q + Or + Ab)$ for the ignimbrites. Green Tuff whole-rock data are from Liszewska et al. [2018] and Williams et al. [2014].

tin [1995] proposed that the differences between the two series were therefore primarily the result of higher fO_2 in the basalt–comendite series most likely due to higher water content, and a similar process was proposed at Changbaishan [Andreeva et al., 2019]. We propose that the same may also be true at Pantelleria.

6. Post-Green Tuff trachyte and pantellerite

Eruption of caldera-filling metaluminous trachyte lavas that comprise the Monte Gibele–Montagna Grande shield volcano followed the eruption of the Green Tuff ignimbrite and collapse of the Cinque Denti caldera (K/Ar 44 ± 8 to 28 ± 16 ka; Cornette et al., 1983, Mahood and Hildreth, 1986). The creation of this intracaldera shield volcano was followed by eruption of pantelleritic trachyte to pantellerite lavas and tuffs, which formed a series of at least 24 coalescing domes, cones, and shields mostly along the rim of, or within, the moat of the caldera from 30–7 ka [Cornette et al., 1983, Mahood and Hildreth, 1986, Scaillet et al., 2011]. The pantellerites are generally similar to those formed during the late stages of formation of the post-caldera trachytes. Some, at least, were compositionally zoned, for example, the Khaggiar lava flow and Randazzo pumices, which can be used to typify this phase of magmatism [Landi and Rotolo, 2015, Neave, 2020, Perugini et al., 2002]. The flow and pumices were erupted at ~8 ka from cones north of Montagna Grande. The compositions range from comenditic trachyte to pantellerite, with overall similarities to the Zinedi Formation (Figure 4b). Neave [2020] has found that there were at least three magma types: trachytes, less evolved pantellerites, and more evolved pantellerites. Compositional variability was generated by accumulation of feldspar into evolved pantellerites, the injection of trachyte magma into less evolved pantellerites and the accumulation of relatively primitive feldspars in trachytic magmas.

Importantly, Neave [2020] proposed that the plumbing system experienced several recharge events prior to eruption and raised the possibility that the three magma types were stored in a com-

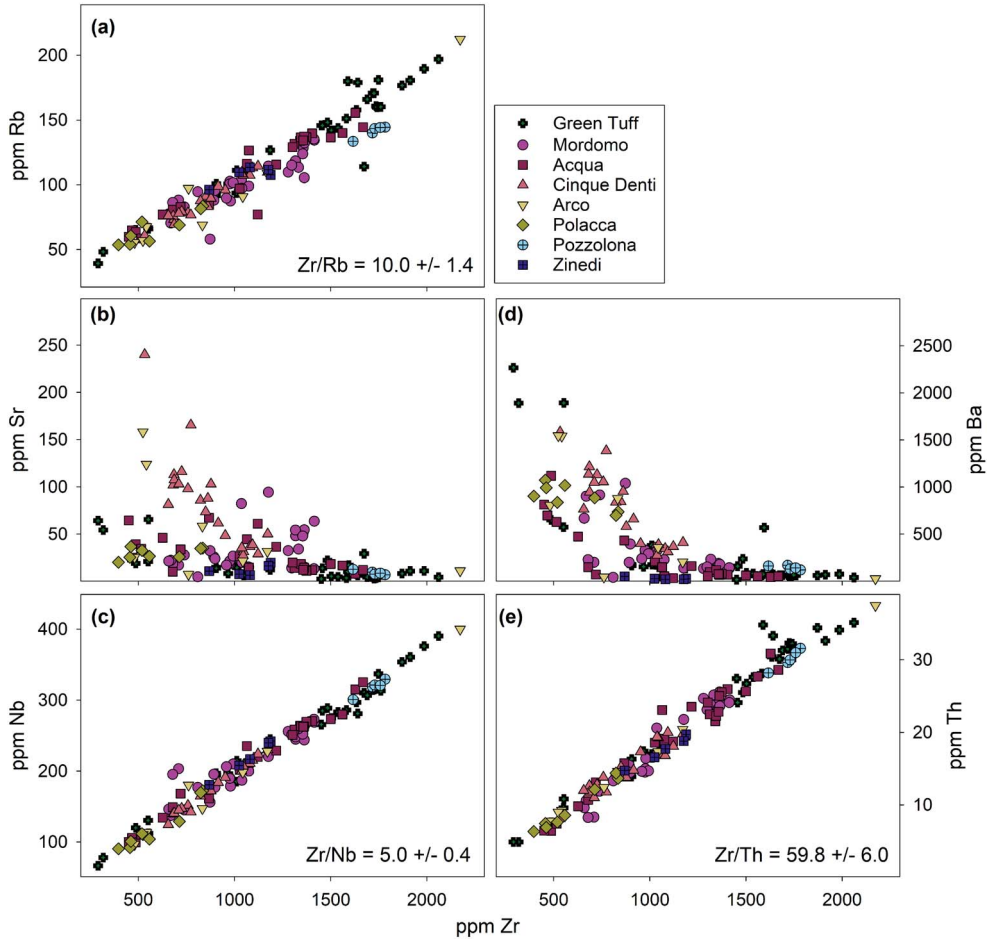

Figure 7. Trace element variation diagrams plotted versus Zr. Incompatible trace element ratios calculated from the entire dataset. Green Tuff whole-rock data are from Liszewska et al. [2018] and Williams et al. [2014].

partmentalized system and followed different LLOD. His cartoon model of the plumbing system comprises an initial stack of three lens-shaped reservoirs connected by dykes. As time progressed, crystal mush erosion connected the upper two reservoirs and the Randazzo and Khaggiar rocks were erupted from this mixed reservoir. The model is in contrast to models of the Green Tuff reservoir, which show a more standard representation of a trachytic mush zone overlain by a stably stratified reservoir zoned from comenditic trachyte to pantellerite [Landi and Rotolo, 2015, Liszewska et al., 2018, Neave et al., 2012]. If the Green Tuff reservoir structure was indeed replaced by another, the change took place in ~13 ka or less. Nonetheless, Neave [2020] stressed that the complexity shown by this small event (<0.1 km^3 DRE) is analogous to that in much bigger peralkaline eruptions, such as the Green Tuff, and in their calc-alkaline counterparts.

Compositional trends for the post-Green Tuff pantellerites are presented in Figure 9. Trachyte lavas are metaluminous to slightly peralkaline (P.I. = 0.90–1.06, with one sample with 1.17 from the "youngest flow" of pantelleritic trachyte on the northeastern flank of Monte Gibele) and silica-saturated to slightly oversaturated (Q* = 0.0–8.75 and 17.8), with Q* values and Zr concentrations consistent with the compositional trends of the Green Tuff. Post-caldera pantellerite lavas generally follow the trend of the Green Tuff Formation, but are characterized by higher P.I., Zr,

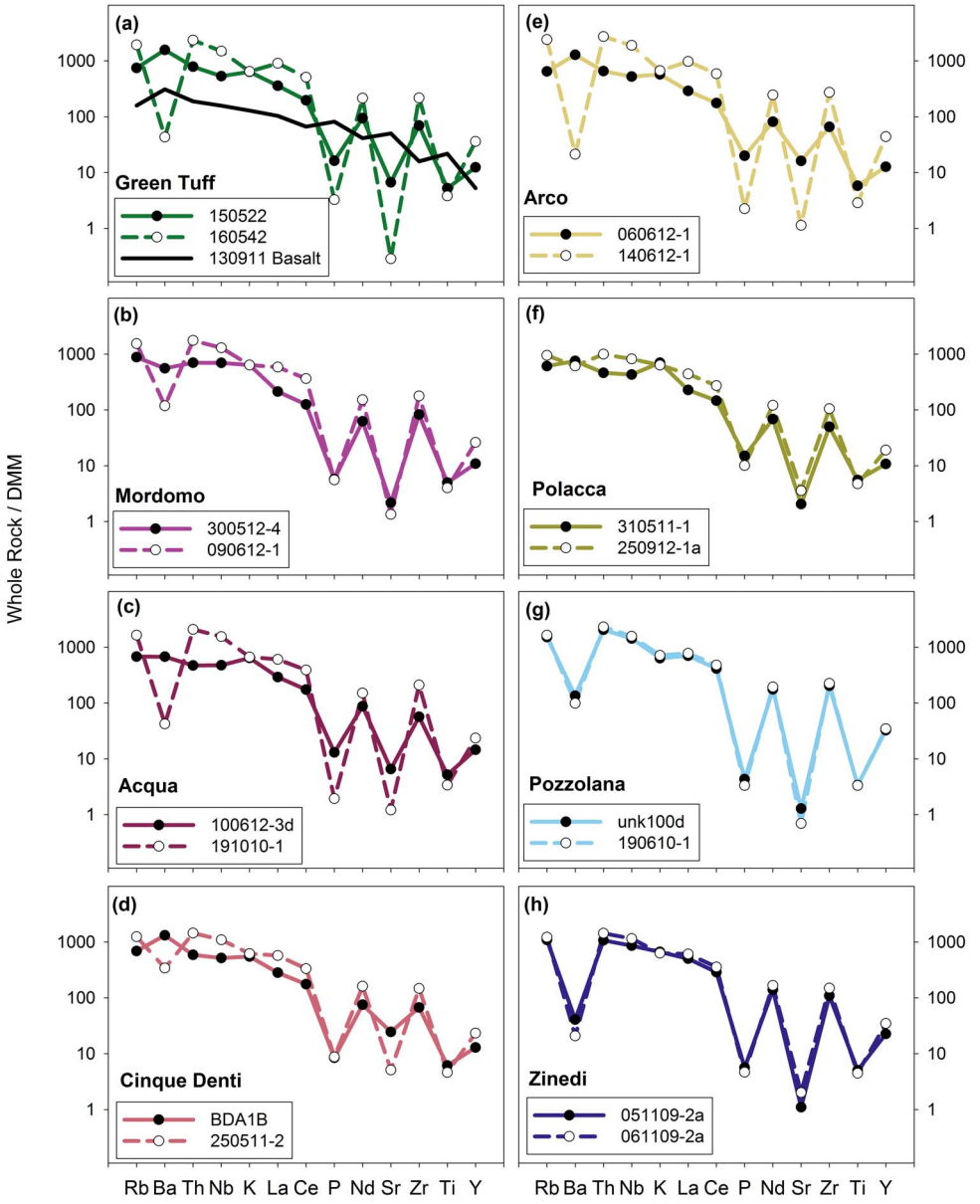

Figure 8. Multi-element variation diagrams normalized to depleted MORB mantle [DMM; Salters and Stracke, 2004] for representative least- and most-evolved samples of each formation (see Table 2). Included with the Green Tuff (a) is a sample of pre-Green Tuff basalt (130911; White et al., 2020) for comparison. Green Tuff data are adapted from Liszewska et al. [2018].

and Q* at a given concentration of SiO_2. Both trends terminate at approximately the same value of Q*, which may imply that these magma reservoirs were stored at similar depths.

As to the future, based on high-precision $^{40}Ar/^{39}Ar$ ages for activity of the past 20 ka, Scaillet et al. [2011] recognized a long-term (>15 ka) decline in eruptive frequency, from 3.5 ka^{-1} to 0.8 ka^{-1}. Combined with geodetic evidence that the caldera floor is deflating and subsiding [De Guidi and Monaco, 2009, Mattia et al., 2007], Scaillet et al. [2011] proposed that the intracaldera system is on the wane, with no evi-

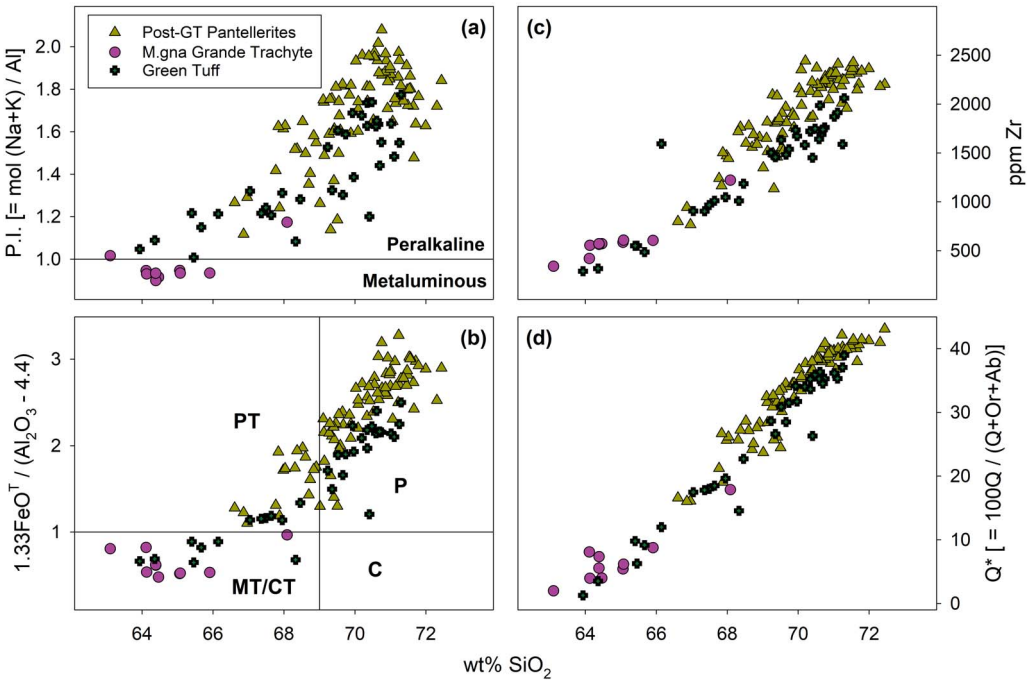

Figure 9. Variation of SiO_2 with (a) the peralkalinity index [P.I.]; (b) relative variability of FeO^T and Al_2O_3 (adapted from Macdonald, 1974); (c) concentration of Zr; and (d) silica-oversaturation, as Q* = 100 · Q/(Q + Or + Ab) for the post-Green Tuff trachytes and pantellerites. Green Tuff whole-rock data are from Liszewska et al. [2018] and Williams et al. [2014]. Other data from Civetta et al. [1984, 1998], Perugini et al. [2002], Avanzinelli et al. [2004], Parker and White [2008], White et al. [2005, 2009], Ferla and Meli [2006], Rotolo et al. [2007].

dence for a forthcoming eruption. However, in noting the similarities between the current period and pre-Green Tuff inter-ignimbrite periods, Jordan et al. [2018] cautioned against assuming that no large, catastrophic eruption will occur in the future, although perhaps not imminently.

The Pantelleria trough, in which the volcano is situated, has high average heat flow (94 ± 21 mW·m^{-2}; Verzhbitsky and Kononov, 2003) and a strong positive Bouguer anomaly (65–103 mGal; Behncke et al., 2006, Civile et al., 2008), features which have been taken to indicate the presence of abundant basaltic magmas at depth [Della Vedova et al., 1995]. Some workers have suggested that there has been asthenospheric upwelling to ~60 km [Argnani and Torelli, 2001, Civile et al., 2008, Della Vedova et al., 1995, White et al., 2020]. Ascent of basaltic magma into the Pantescan reservoir, perhaps promoted by increased tensional regional stresses, could result in renewed silicic magmatism.

7. Conclusions

(1) From ~190 to 46 ka, the Pantescan plumbing system erupted eight ignimbritic formations from what is inferred to have been a stably stratified reservoir.
(2) The earliest ignimbrite (Zinedi Fm.) was pantelleritic whereas later ignimbrites had comenditic affinities.
(3) The Green Tuff eruption at 45.7 ± 1.0 ka, which produced the ninth and last ignimbrite, was apparently considerably more complex than earlier activity, ranging from metaluminous trachytes to pantellerites. It was immediately followed by a suite of trachytes taken to represent a mush zone in the reservoir.
(4) Magmatism from 25–7 ka was dominated by pantellerites broadly similar in composition to those of the oldest ignimbrite. The upper

part of the plumbing system has shown signs of increasingly open system behaviour.

(5) All felsic series evolved from a similar basaltic parent along similar LLOD leading to trachyte, with differences in both pressure (depth of the reservoir) and oxygen fugacity (possibly linked to water content) contributing to whether the trachyte evolved to comendite (under higher pressures and more oxidizing conditions) or to pantellerite (under lower pressures and more reducing conditions). Detailed petrogenetic studies of these older comendite units are necessary and ongoing.

Acknowledgements

NJJ gratefully acknowledges funding from the German Academic Exchange Service, Geological Society of London, Mineralogical Society of Great Britain and Ireland, Geologists' Association, Quaternary Research Association, Volcanic and Magmatic Studies Group, and the Department of Geology at the University of Leicester. We wish to thank Raffaello Cioni and an anonymous reviewer for their helpful comments.

Supplementary data

Supporting information for this article is available on the journal's website under https://doi.org/10.5802/crgeos.50 or from the author.

References

Andreeva, O. A., Andreeva, I. A., and Yarmolyuk, V. V. (2019). Effect of redox conditions of the evolution of magmas of Changbaishan Tianchi volcano, China–North Korea. *Chem. Geol.*, 508, 225–233.

Argnani, A. and Torelli, L. (2001). The Pelagian Shelf and its graben system (Italy/Tunisia). In Ziegler, P. A., Cavassa, W., Robertson, A. H. F., and Crasquin-Soleau, S., editors, *Peri-Tethys Memoir 6: Peri-Tethyan Rift/Wrench Basins and Passive Margins*, volume 186 of *Mem. Mus. Natl. Hist. Nat.*, pages 529–544. Editions du Musém, Paris.

Avanzinelli, R., Bindi, L., Menchetti, S., and Conticelli, S. (2004). Crystallization and genesis of peralkaline magmas from Pantelleria Volcano, Italy: an integrated petrological and crystal-chemical study. *Lithos*, 73, 41–69.

Bagiński, B., Macdonald, R., White, J. C., and Jeżak, L. (2018). Tuhualite in a peralkaline rhyolitic ignimbrite from Pantelleria, Italy. *Eur. J. Mineral.*, 30, 367–373.

Behncke, B., Berrino, G., Corrado, G., and Velardita, R. (2006). Ground deformation and gravity changes on the island of Pantelleria in the geodynamic framework of the Sicily Channel. *J. Volcanol. Geotherm. Res.*, 150, 146–162.

Civetta, L., Cornette, Y., Crisci, G. M., Gillot, P. Y., Orsi, G., and Requejo, C. S. (1984). Geology, geochronology and chemical evolution of the island of Pantelleria. *Geol. Mag.*, 121, 541–668.

Civetta, L., Cornette, Y., Gillot, P. Y., and Orsi, G. (1988). The eruptive history of Pantelleria (Sicily Channel) in the last 50 ka. *Bull. Volcanol.*, 50, 47–57.

Civetta, L., D'Antonio, M., Orsi, G., and Tilton, G. R. (1998). The geochemistry of volcanic rocks from Pantelleria island, Sicily Channel: petrogenesis and characteristics of the mantle source region. *J. Petrol.*, 39, 1453–1491.

Civile, D., Lodolo, E., Tortorici, L., Lanzafame, G., and Brancolini, G. (2008). Relationships between magmatism and tectonics in a continental rift: the Pantelleria Island region (Sicily Channel, Italy). *Marine Geol.*, 251, 32–46.

Cornette, Y., Crisci, G. M., Gillot, P. Y., and Orsi, G. (1983). Recent volcanic history of Pantelleria: a new interpretation. *J. Volcanol. Geotherm. Res.*, 17, 361–373.

De Guidi, G. and Monaco, C. (2009). Late Holocene vertical deformation along the coast of Pantelleria Island (Sicily Channel, Italy). *Quat. Internat.*, 206, 158–165.

Della Vedova, B., Lucazeau, F., Pasquale, V., Pellis, G., and Verdoya, M. (1995). Heat flow in the tectonic provinces crossed by the southern segment of the European Geotraverse. *Tectonophysics*, 244, 57–74.

Di Carlo, I., Rotolo, S., Scaillet, B., Buccheri, V., and Pichavant, M. (2010). Phase equilibrium constraints on pre-eruptive conditions of recent explosive volcanism of Pantelleria Island, Italy. *J. Petrol.*, 51, 2245–2276.

Ferla, P. and Meli, C. (2006). Evidence of magma mix-

ing in the 'Daly Gap' of alkaline suites: a case study from the enclaves of Pantelleria (Italy). *J. Petrol.*, 47, 1467–1502.

Gianelli, G. and Grassi, S. (2001). Water-rock interaction in the active geothermal system of Pantelleria, Italy. *Chem. Geol.*, 181, 113–130.

Giuffrida, M., Nicotra, E., and Viccaro, M. (2020). Changing modes and rates of mafic magma supply at Pantelleria (Sicily Channel, Southern Italy): new perspectives on the volcano factory drawn upon olivine records. *J. Petrol.*, 61, 1–22.

Ishihara, S. (1977). The magnetite-series and ilmenite-series granitic rocks. *Mining Geol.*, 27, 293–305.

Jochum, K. P., Nohl, U., Herwig, K., Lammel, E., Stoll, B., and Hofmann, A. W. (2007). GeoReM: A new geochemical database for reference materials and isotopic standards. Geostand. *Geoanal. Res.*, 29, 333–338.

Johannes, W. and Holtz, F. (1996). The haplogranite system Qz–Ab–Or. In Johannes, W. and Holtz, F., editors, *Petrogenesis and Experimental Petrology of Granitic Rocks*, pages 18–57. Springer, London.

Jordan, N. J. (2014). *Pre-Green Tuff explosive eruptive history, petrogenesis and proximal-distal tephra correlations of a peralkaline caldera volcano: Pantelleria, Italy*. PhD thesis, University of Leicester, UK.

Jordan, N. J., Rotolo, S. G., Williams, R., Speranza, F., McIntosh, W. C., Branney, M. J., and Scaillet, S. (2018). Explosive eruptive history of Pantelleria, Italy: Repeated caldera collapse and ignimbrite emplacement at a peralkaline volcano. *J. Volcanol. Geotherm. Res.*, 349, 47–73.

Kelsey, C. H. (1965). Calculation of the C.I.P.W. norm. *Mineral. Mag.*, 34, 276–282.

Landi, P. and Rotolo, S. G. (2015). Cooling and crystallization recorded in trachytic enclaves hosted in pantelleritic magmas (Pantelleria, Italy): Implications for pantellerite genesis. *J. Volcanol. Geotherm. Res.*, 301, 169–179.

Lanzo, G., Landi, P., and Rotolo, S. G. (2013). Volatiles in pantellerite magmas: A case study of the Green Tuff Plinian eruption (Island of Pantelleria, Italy). *J. Volcanol. Geotherm. Res.*, 262, 153–163.

Le Maitre, R. W. (1976). Some problems of the projection of chemical data into mineralogical classifications. *Contrib. Mineral. Petrol.*, 56, 181–189.

Le Maitre, R. W., editor (2002). *Igneous Rocks, a Classification and Glossary of Terms: Recommendations of the International Union of Geological Sciences Subcomission on the Systematics of Igneous Rocks*. Cambridge University Press, Cambridge, UK, 2nd edition. 236 p.

Liszewska, K. M., White, J. C., Macdonald, R., and Bagiński, B. (2018). Compositional and thermodynamic variability in a stratified magma chamber: Evidence from the Green Tuff Ignimbrite (Pantelleria, Italy). *J. Petrol.*, 59, 2245–2272.

Macdonald, R. (1974). Nomenclature and petrochemistry of the peralkaline oversaturated extrusive rocks. *Bull. Volcanol.*, 38, 498–516.

Mahood, G. A. and Hildreth, W. (1986). Geology of the peralkaline volcano at Pantelleria, Strait of Sicily. *Bull. Volcanol.*, 48, 143–172.

Mattia, M., Bonaccorso, A., and Guglielmino, F. (2007). Ground deformations in the Island of Pantelleria (Italy): Insights into the dynamics of the current intereruptive period. *J. Geophys. Res.*, 112, article no. B11406.

Mungall, J. E. and Martin, R. F. (1995). Petrogenesis of basalt-comendite and basalt-pantellerite series, Terceira, Azores, and some implications for the origin of ocean-island rhyolites. *Contrib. Mineral. Petrol.*, 119, 43–55.

Neave, D. A. (2020). Chemical variability in peralkaline magmas and magma reservoirs: insights from the Khaggiar lava flow, Pantelleria, Italy. *Contrib. Mineral. Petrol.*, 175, article no. 39.

Neave, D. A., Fabbro, G., Herd, R. A., Petrone, C. M., and Edmonds, M. (2012). Melting, differentiation and degassing at the Pantelleria volcano, Italy. *J. Petrol.*, 53, 637–663.

Nicholls, J., Carmichael, I. S. E., and Stormer Jr., J. C. (1971). Silica activity and P_{total} in igneous rocks. *Contrib. Mineral. Petrol.*, 33, 1–20.

Parker, D. F. and White, J. C. (2008). Large-scale alkalic magmatism associated with the Buckhorn caldera, Trans-Pecos Texas, USA: Comparison with Pantelleria, Italy. *Bull. Volcanol.*, 70, 403–415.

Perugini, D., Poli, G., and Prosperini, N. (2002). Morphometric analysis of magmatic enclaves: a tool for understanding magma vesiculation and ascent. *Lithos*, 61, 225–235.

Romano, P., Andújar, J., Scaillet, B., Romengo, N., Di Carlo, I., and Rotolo, S. G. (2018). Phase equilibria of Pantelleria trachytes (Italy): constraints on pre-eruptive conditions and on the metaluminous to peralkaline transition in silicic magmas. *J. Petrol.*, 59, 559–588.

Romano, P., Scaillet, B., White, J. C., Andújar, J., Di Carlo, I., and Rotolo, S. G. (2020). Experimental and thermodynamic constraints on mineral equilibrium in pantelleritic magmas. *Lithos*, 376–377, article no. 105793.

Romano, P., White, J. C., Ciulla, A., Di Carlo, I., D'Oriano, C., Landi, P., and Rotolo, S. G. (2019). Volatiles and trace elements content in melt inclusions from the zoned Green Tuff ignimbrite (Pantelleria, Sicily): petrological inferences. *Ann. Geophys.*, 62, article no. VO09.

Romengo, N., Landi, P., and Rotolo, S. G. (2012). Evidence of basaltic magma intrusions in a trachytic magma chamber at Pantelleria (Italy). *Period. Mineral.*, 81, 163–178.

Ronga, F., Lustrino, M., Marzoli, A., and Melluso, L. (2009). Petrogenesis of a basalt-comendite-pantellerite rock suite: the Boseti volcanic complex (main Ethiopian rift). *Mineral. Petrol.*, 98, 227–243.

Rotolo, S. G., La Felice, S., Mangalaviti, A., and Landi, P. (2007). Petrology and geochemistry of the recent (<25 ka) silicic volcanism at Pantelleria island. *Boll. Soc. Geol. Ital.*, 126, 191–208.

Rotolo, S. G., Scaillet, S., La Felice, S. L., and Vita-Scaillet, G. (2013). A revision of the structure and stratigraphy of pre-Green Tuff ignimbrites at Pantelleria (Strait of Sicily). *J. Volcanol. Geotherm. Res.*, 250, 61–74.

Rotolo, S. G., Scaillet, S., Speranza, F., White, J. C., Williams, R., and Jordan, N. J. (2021). Volcanological evolution of Pantelleria Island (Strait of Sicily) peralkaline volcano: a review. *C. R. Geosci.*, 353(S2), 111–132.

Rotolo, S. G. and Villa, L. M. (2001). ^{39}Ar–^{40}Ar dating of an alkali-granite enclave from Pantelleria. *Period. Mineral.*, 70, 269–275.

Salters, V. J. M. and Stracke, A. (2004). Composition of depleted mantle. *Geochem. Geophys. Geosyst.*, 5, article no. Q05004.

Scaillet, S., Rotolo, S. G., La Felice, S., and Vita-Scaillet, G. (2011). High-resolution ^{40}Ar/^{39}Ar chronostratigraphy of the post-caldera (<20 ka) volcanic activity at Pantelleria, Sicily Strait. *Earth Planet. Sci. Lett.*, 309, 280–290.

Scaillet, S., Vita-Scaillet, G., and Rotolo, S. G. (2013). Millenial-scale phase relationships between ice-core and Mediterranean marine records: insights from high-precision ^{40}Ar/^{39}Ar dating of the Green Tuff of Pantelleria, Sicily Strait. *Quat. Sci. Rev.*, 78, 141–154.

Speranza, F., Di Chiara, A., and Rotolo, S. G. (2012). Correlation of welded ignimbrites on Pantelleria (Strait of Sicily) using paleomagnetism. *Bull. Volcanol.*, 74, 341–357.

Stabile, P., Giuli, G., Cicconi, M. R., Paris, E., Trapananti, A., and Behrens, H. (2017). The effect of oxygen fugacity and Na/(Na+K) ratio on iron speciation in pantelleritc glasses. *J. Non-Cryst. Solids*, 478, 65–74.

Toplis, M. J. and Carroll, M. R. (1995). An experimental study of the influence of oxygen fugacity on Fe-Ti oxide stability, phase relations, and mineral-melt equilibria in ferro-basaltic systems. *J. Petrol.*, 36, 1137–1170.

Tuttle, O. F. and Bowen, N. L. (1958). *Origin of granite in light of experimental studies in the system $NaAlSi_3O_8$–$KAlSi_3O_8$–SiO_2–H_2O*, volume 74 of *GSA Memoirs*. Geological Society of America.

Verzhbitsky, E. V. and Kononov, M. V. (2003). Heat flow and origin of the lithosphere in the central Mediterranean region. *Geotectonics*, 37, 328–336.

White, J. C., Neave, D. A., Rotolo, S. G., and Parker, D. F. (2020). Geochemical constraints on basalt petrogenesis in the Strait of Sicily Rift Zone (Italy): Insights into the importance of short lengthscale mantle heterogeneity. *Chem. Geol.*, 545, article no. 119650.

White, J. C., Parker, D. F., and Ren, M. (2009). The origin of trachyte and pantellerite from Pantelleria, Italy: Insights from major element, trace element, and thermodynamic modelling. *J. Volcanol. Geotherm. Res.*, 179, 33–55.

White, J. C., Ren, M., and Parker, D. F. (2005). Variation in mineralogy, temperature, and oxygen fugacity in a suite of strongly peralkaline lavas and tuffs, Pantelleria, Italy. *Can. Mineral.*, 43, 1331–1347.

Wilke, S., Holtz, F., Neave, D. A., and Almeev, R. (2017). The effect of anorthite content and wa-

ter on quartz-feldspar cotectic compositions in the rhyolitic system and implications for geobarometry. *J. Petrol.*, 58, 789–818.

Williams, R., Branney, M. J., and Barry, T. L. (2014). Temporal and spatial evolution of a waxing then waning catastrophic density current revealed by chemical mapping. *Geology*, 42, 107–110.